SUPPLEMENTARY INFORMATION:

NANOSCALE MORPHOLOGICAL AND CHEMICAL CHANGES OF HIGH VOLTAGE LITHIUM-MANGANESE RICH NMC COMPOSITE CATHODES WITH CYCLING

Feifei Yang, Yijin Liu, Surendra K. Martha, Ziyu Wu, Joy C. Andrews, Gene E. Ice, Piero Pianetta, Jagjit Nanda

MATERIAL AND ELECTROCHEMICAL CYCLING

LMR-NMC cathode powders with nominal composition $Li_{1.2}Mn_{0.525}Ni_{0.175}Co_{0.1}O_2$ were obtained from Toda Kogyo Corporation's pilot scale facility in Japan. These particles have spherical aggregated morphologies in the size range between 4-12 microns, as shown in Fig. S1 (left) below. The primary cathode particles are faceted, with average size ~ 100 nm (Fig. S1 (right)).

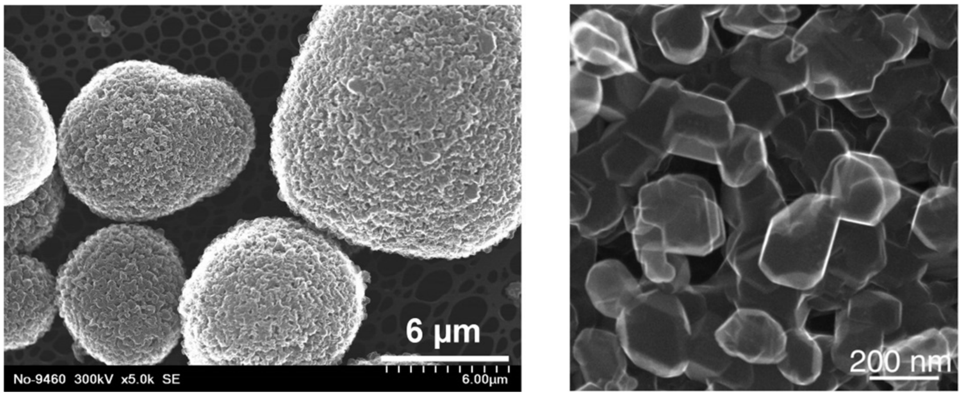

Fig. S1. The morphology of pristine Li-Mn-rich NMC particles was characterized using a Hitachi S-4800 scanning electron microscope (Hitachi High Technologies America, Inc., USA). (**Left**) Secondary particles having spherical morphology with typical particle diameters ranging between 4-12 µm. (**Right**) Higher magnification images show primary particles with faceted surfaces in the size range of ~100 nm.

A series of battery electrode samples were recovered at different stages of the battery life time (pristine, 1 cycle, 50 cycles and 200 cycles). The electrode samples were stored/transported/handled in an Ar glove box to prevent the sample from oxygen damage/contamination. The methods used for cell assembly and electrochemical measurements are described elsewhere[1]. Galvanostatic charge–discharge cycling was carried out using a multichannel battery tester (model 4000, Maccor Inc., USA) in two-electrode coin-type cells. The cells were discharged galvanostatically at C/10 rate followed by galvanostatic charging at C/10 rate to 4.9 V followed by potentiostatic charge until the current reaches C/50.The differential capacity (dq/dv) versus voltage plot for the 1st, 50th and 200 cycles is shown in Fig. S2.

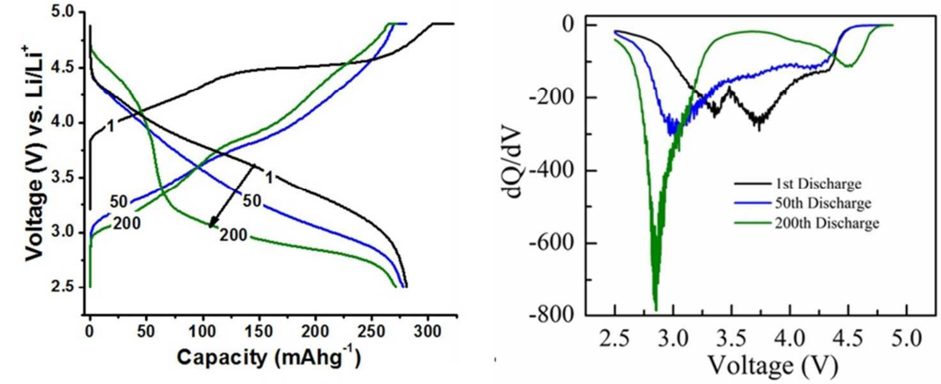

Fig. S2. Left: Charge-discharge voltage profile of LMR-NMC cathode at various stages of cycling. Right: Differential capacity (dq/dv) versus voltage plot for the 1st, 50th and 200 cycles.

MICROSCOPY

We performed hard X-ray full-field (FF) transmission X-ray microscopy (TXM) on the battery electrodes at beamline 6-2C of the Stanford Synchrotron Radiation Lightsource (SSRL) at the SLAC National Accelerator Laboratory. The TXM at SSRL operates over an energy range of ~4.5 keV to 13 keV, covering the K-edges of the transition metals (Mn, Co, and Ni) included in the investigated battery electrode. The objective zoneplate provides 50X magnification in addition to the optical objective lens, enabling a spatial resolution of ~30 nm. More details of the hardware configuration can be found elsewhere[2]. The Fresnel zoneplate is automatically refocused as the energy of the incident X-rays is adjusted, causing slight differences in magnification. The sample translation in a plane perpendicular to the X-ray direction was also combined (mosaic tomography) in order to increase the field of view. Image preprocessing including magnification correction, mosaic tile stitching, motor jitter correction, and image registration were performed using an in-house developed software package, TXM-Wizard[3]. The automatic image registration is critical to the evaluation of the energy dependence of the projection images and the 3D volumes; and thus Phase Correlation, Cross Correlation, and SIFT algorithms[3]were employed in this study, showing no significant differences. It's worth mentioning that the spatial resolution of the X-ray microscopy techniques is usually set by the quality of the X-ray focusing optics (we refer to two nice review articles by Sakdinawat *et al.*[4] and by Yan *et al.*[5] for more details).

TWO DIMENSIONAL TXM-XANES

2D FF TXM-XANES[6] was conducted over the absorption edges of all three Transition Metals (Mn, Co, and Ni) (images taken at >85 energy points across each X-ray absorption K-edge). The energy was calibrated to literature values[7] e.g. by fitting of the pre-edge peak in the MnO_2 spectrum. When comparing bulk FF TXM-XANES data (averaged over the entire illuminated field of view) of the pristine and 200×-cycle samples, the near edge spectroscopic data over the Mn K-edge showed the most pronounced differences (see Fig. 1a and Fig. S3) and were chosen to be the key fingerprints for studying the chemical phase transition. The two extreme spectra were used as standard spectra (the two principle components) to perform linear combination fitting of each single-pixel XANES for all samples with different numbers of battery cycles. A magnified view of the pre-edge to white line region of the spectra is shown in the inset of Fig. S3. The spectra in Fig. S3 are color coded to the images shown in Figs. 1A to 1D and to Fig. S4, which shows two more 2D chemical maps of the 50×-cycled particles at randomly selected locations on the electrode. The similarity between Fig. S4 and Fig. 1C indicates that the investigated areas are representative of Mn speciation in the electrode.

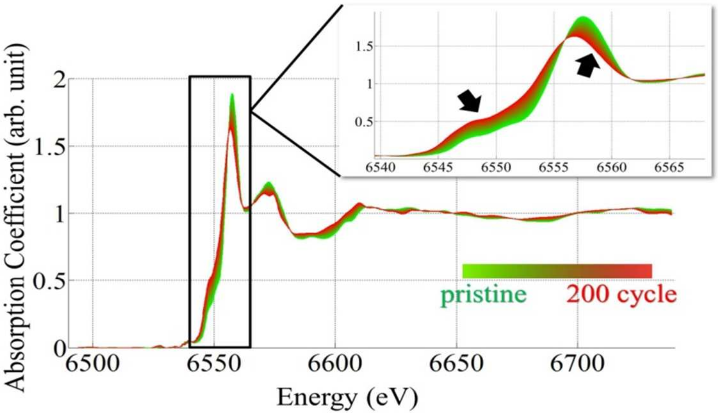

Fig. S3. The bulk spectroscopic data (added from single-pixel XANES) over the Mn K-edge for the pristine and the 200×-cycle LMR-NMC battery electrodes, measured at SSRL beamline 6-2C. A magnified view of the pre-edge to white line region of the spectra (the highlighted energy window) is plotted in the inset.

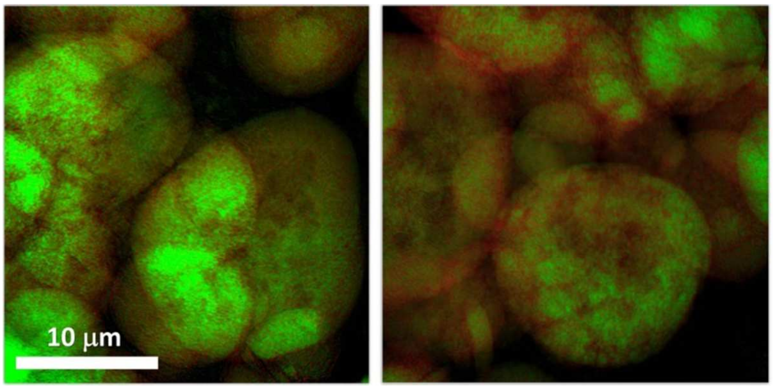

Fig. S4. Two chemical maps of 50×-cycled particles at randomly selected locations on the electrode. The scale bar in the figure is 10 microns. The similarity of these two maps and those in Fig. 1C demonstrates that the investigated area is representative of the overall Mn chemical distribution.

THREE DIMENSIONAL EVALUATIONS

Tomography was also carried out at multiple X-ray energies (6510 eV, 6630 eV, 7680 eV, 7800 eV, 8300 eV and 8380 eV; above and below the absorption K-edges of Mn, Co and Ni, respectively) for the as-made (pristine) sample as well as sample recovered after one and 200 charge-discharge cycles. The reconstructed volumes at different energies show the energy dependence of the absorption coefficient spatially resolved at each voxel over the 3D volume, and thus provide 3D elemental sensitivity. In the tomography scan, images were taken at 181 viewing angles (-90° to 90° with 1° step). Iterative tomographic reconstruction was adopted to increase the signal to noise ratio in the reconstructed 3D volumes[8,9]. The sample translation in a plane perpendicular to the X-ray direction was also combined (mosaic tomography) in order to increase the field of view. Image registration and correction were performed using an in-house software package, TXM-Wizard[3].

We define the averaged relative elemental concentration (AREC; plotted versus the depth of the pixel layers in Fig.5) using the formula $AREC(L) = (TM_L/TM_{all})/(Nvoxel_L/Nvoxel_{all})$; in which L is the index of the pixel layers, TM is the amount of the transition metal (Mn, Co, or Ni), and *Nvoxels* is the number of voxels. Plotting this unitless parameter as a function of L provides a measurement of the uniformity in the depth dependency, with a value of 1 indicating uniform composition (independent of depth).

Additional References for supplementary material

1. McCalla, E.; Rowe, A. W.; Shunmugasundaram, R.; Dahn, J. R. *Chem. Mater.* **2013,** 25, 989.
2. Nelson, J.; Misra, S.; Yang, Y.; Jackson, A.; Liu, Y.; Wang, H.; Dai, H.; Andrews, J. C.; Cui, Y.; Toney, M. F. *J. Am. Chem. Soc.* **2012,** 134, 6337.
3. Liu, Y.; Meirer, F.; Williams, P. A.; Wang, J.; Andrews, J. C.; Pianetta, P. *Journal of Synchrotron Radiation* **2012,** 19, 281.
4. Sakdinawat, A.; Attwood, D. *Nature Photonics* **2010**, 4, 840.
5. Yan, H.; Conley, R.; Bouet, N.; Chu, Y. S. *Journal of Physics D: Applied Physics* **2014**, 47, 263001.
6. Meirer, F.; Cabana, J.; Liu, Y.; Mehta, A.; Andrews, J. C.; Pianetta, P. *J. Synchr. Radiat.* **2011,** 18, 773.
7. Croft, M.; Sills, D.; Greenblatt, M.; Lee, C.; Cheong, S. W.; Ramanujachary, K. V.; Tran, D. *Phys. Rev. B* **1997,** 55, 8726.
8. Liu, Y.; Meirer, F.; Wang, J.; Requena, G.; Williams, P.; Nelson, J.; Mehta, A.; Andrews, J. C.; Pianetta, P. *Anal. Bioanal. Chem.* **2012,** 404, 1297.
9. Wang, J.; Yang, W.; Wang, S.; Xiao, X.; De Carlo, F.; Liu, Y.; Mao, W. L. *Journal of Applied Physics* **2012,** 111, 112626.